conference papers

Solution structure of Ca^{2+}/calmodulin complexed with a lentivirus lytic peptide 1 reveals a novel mode of molecular recognition

Yoshinobu Izumi,* Akira Amano, Takeshi Saito and Yuji Jinbo

Graduate Program of Human Sensing and Sensor Engineering, Graduate School of Science and Engineering, Yamagata University, Johnan 4-3-16, Yonezawa, Yamagata 992-8510, Japan. Correspondence e-mail: yizumi@yz.yamagata-u.ac.jp

Small-angle X-ray scattering was used to analyze the interaction of Ca^{2+}/calmodulin (CaM) with a lentivirus lytic peptide 1 (LLP1) derived from the cytoplasmic tail of HIV-1 transmembrane glycoprotein. The synthetic peptide homologues of LLP1 were selected from three species of the glycoprotein: ENV_HV1A2, ENV_HV1B1 and ENV_HV1H2. Ca^{2+}/CaM binds LLP1 with the truncation of three or ten residues and adopts almost the same globular structure as that of the complex with a peptide from myosin light chain kinase (MLCK), indicating that the Ca^{2+}/CaM-binding site locates on the shorter sequence. Moreover, Ca^{2+}/CaM binds a peptide with the opposite sequence and adopts almost the same globular structure as that in the original sequence. Taken together, the results provide evidence that LLP1 can bind to the N- and C-terminal lobes of CaM with a polarity opposite to that observed for the CaM–MLCK complex and the binding mode of Ca^{2+}/CaM molecular recognition is well preserved despite the sequence variation in the three species, suggesting that this region of the transmembrane glycoprotein is important to viral replication.

1. Introduction

The human immunodeficiency virus type 1 (HIV-1) envelope gp160 comprises a surface domain (gp120) and a transmembrane domain (gp41). Both are required for viral entry into the cell. The gp41 is organized into three major regions: an extracellular (N-terminal) ectodomain, a transmembrane segment and a C-terminal cytoplasmic tail. The latter has been shown to provide several important functions, including virus replication, infectivity, transmission and cytopathogenicity in the virus life cycle. It contains two amphipathic regions: lentiviral lytic peptide (LLP) 1 and LLP2 (Miller *et al.*, 1991), which bind the ubiquitous Ca^{2+}-binding protein calmodulin (CaM) and inhibit its activation of enzymes (Miller *et al.*, 1993; Srinivas *et al.*, 1993). Of the lytic and CaM-binding properties of the LLPs, inhibition of cellular CaM is of particular interest with regard to possible mechanisms of HIV-1 pathogenesis. As the Ca^{2+}-saturated CaM (Ca^{2+}/CaM) response cascade is an essential component for activation of T cell populations and plays an important role in many other cellular processes, subversion of CaM to a nonproductive viral target may have important detrimental consequences to host cell proliferation pathways. Thus, the uncoupling of Ca^{2+}-dependent signal transduction pathways of targeted lymphocyte populations may play a role in immunosuppression.

Previous studies have shown that the CaM-binding function is well preserved despite the sequence variation observed in nature (Tencza *et al.*, 1997). However, it is still not known what mode of molecular recognition can be applied to the present CaM-target interactions. In the present study, small-angle X-ray scattering (SAXS) was used to analyze the interactions of Ca^{2+}/CaM with LLP1. The results indicate that LLP1 binds the N- and C-terminal lobes of CaM with a polarity

opposite to that observed for the CaM–MLCK peptide complex and that the binding mode of Ca^{2+}/CaM molecular recognition is well preserved despite the sequence variation in the three species, suggesting that this region of the gp41 is important to viral replication.

2. Materials and methods

2.1. Materials

The recombinant rat CaM was expressed in *Escherichia coli* and purified to homogeneity as described previously (Hayashi *et al.*, 1998). The LLP1s were selected from ENV_HV1A2 (aa 836–855; HV1A2), ENV_HV1B1 (aa 837–856; HV1B1) and ENV_HV1H2 (aa 837–856; HV1H2), synthesized on an Applied Biosystems Model 431A peptide synthesizer using the general procedure and purified by reverse high performance liquid chromatography as described previously (Izumi *et al.*, 2001). Two CaM-binding domains of skeletal and smooth muscle light chain kinase (skMLCK and smMLCK, respectively) were used as a canonical peptide for the determination of the molecular recognition motif (Ikura *et al.*, 1992; Meador *et al.*, 1992). Fig. 1 summarizes the primary sequences of synthetic LLP1s and MLCK peptide, in which Δ represents the truncation of amino-acid residues from the C terminus. For SAXS experiments, the recombinant CaM was dissolved in Tris buffer (50 m*M* Tris–HCl, pH 7.6) containing 120 m*M* NaCl. A complex of Ca^{2+}/CaM with MLCK peptide or each peptide of LLP1 was prepared by mixing the protein with both a 4.4-fold molar excess of Ca^{2+} and a 1.1-fold molar excess of each peptide. The protein concentrations for Ca^{2+}/CaM/LLP1 were 5.0, 7.5, 10.0, 12.5, 15.0 and 17.5 mg ml^{-1}, while those for Ca^{2+}/CaM/

Figure 1

Peptide name	Primary sequence	aa
HV1A2	DRVIEVVQGAYRAILHIHRRIRQGLERILL	30
HV1A2Δ3	DRVIEVVQGAYRAILHIHRRIRQGLER	27
HV1A2Δ10	DRVIEVVQGAYRAILHIHRR	20
HV1B1Δ10	DRVIEVVQGAYRAIRHIPRR	20
HV1H2Δ10	DRVIEVVQGACRAIRHIPRR	20
HV1H2WΔ10	DRVIEVVQGWCRAIRHIPRR	20
HV1rA2Δ10	RRHIHLIARYARQAVEIVRD	20
smMLCK	RRKWQKTGHAVRAIGRLSSS	20
skMLCK	KKRWKKNFIAVSAANRFKKISS	22

Primary sequences of the synthetic peptides used in this study. aa represents the number of amino acids. Acidic, basic, hydrophilic and hydrophobic residues are shown in red, blue, black and green, respectively. Abbreviations for the amino-acid residues are: A, Ala; C, Cys; D, Asp; E, Glu; F, Phe; G, Gly; H, His; I, Ile; K, Lys; L, Leu; M, Met; N, Asn; P, Pro; Q, Glu; R, Arg; S, Ser; T, Thr; V, Val; W, Trp; and Y, Tyr.

Table 1

M_{SAXS}/M_{cal} and second virial coefficient (A_2), radius of gyration at infinite dilution (R_0) and parameter of interparticle interference (B_{if}) for Ca^{2+}/CaM/peptide at pH 7.6.

Protein	M_{SAXS}/M_{cal}†	A_2 (10^{-4} mol cm^3 g^{-2})	R_0 (Å)	B_{if} (10^{-13} cm^5 g^{-1})
Ca^{2+}/CaM	1.00	3.3 ± 0.3	21.6 ± 0.3	2.7 ± 0.3
Ca^{2+}/CaM/smMLCK	1.00	5.4 ± 0.3	18.0 ± 0.3	2.5 ± 0.3
Ca^{2+}/CaM/skMLCK	1.00	2.3 ± 0.2	18.0 ± 0.3	1.0 ± 0.3
Ca^{2+}/CaM/HV1A2Δ3	1.07 ± 0.07	−0.1 ± 0.3	18.5 ± 0.4	−2.0 ± 0.4
Ca^{2+}/CaM/HV1A2Δ10	1.02 ± 0.05	3.1 ± 0.3	18.9 ± 0.3	2.6 ± 0.3
Ca^{2+}/CaM/HV1rA2Δ10	0.98 ± 0.05	2.5 ± 0.2	19.3 ± 0.3	1.9 ± 0.2
Ca^{2+}/CaM/HV1B1Δ10	1.04 ± 0.05	3.6 ± 0.3	19.1 ± 0.3	2.7 ± 0.3
Ca^{2+}/CaM/HV1H2Δ10	1.04 ± 0.05	2.9 ± 0.3	19.8 ± 0.3	3.5 ± 0.3
Ca^{2+}/CaM/HV1H2WΔ10	1.09 ± 0.09	4.3 ± 0.3	19.6 ± 0.3	3.2 ± 0.3

† Ratio of the molecular weight of a Ca^{2+}/CaM/peptide complex to the calculated value.

MLCK peptide were 7.5, 10.0, 12.5, 15.0, 17.5 and 20.0 mg ml^{-1}. The concentration of the proteins was determined as described previously (Lowry *et al.*, 1951).

2.2. SAXS measurements

The measurements were performed using synchrotron orbital radiation with an instrument for SAXS installed at BL-10C of the Photon Factory, KEK, Tsukuba, Japan (Ueki *et al.*, 1985). An X-ray wavelength of 1.488 Å was selected. The temperature of the SAXS experiment was kept at 298.15 ± 0.05 K by circulating water through the cell holder. The reciprocal parameter, s, equal to $(2\sin\theta)/\lambda$, was calibrated by the observation of a diffraction pattern from chicken collagen, where 2θ is the scattering angle and λ is the X-ray wavelength. Scattering data were collected for 300 s at various protein concentrations.

2.3. SAXS analyses

Two methods of data analysis were used. The first method was that of Guinier & Fournet (1955). The scattering intensity $I(s, c)$ measured as a function of s at a finite protein concentration c is given by

$$I(s, c) = I(0, c)\exp[-(4\pi^2/3)R_g(c)^2 s^2], \tag{1}$$

where $I(0, c)$ is the scattering intensity at $s = 0$ and $R_g(c)$ is the radius of gyration at a concentration c. In the dilute limit, $I(0, c)$ is given by

$$Kc/I(0, c) = 1/M + 2A_2 c + \ldots, \tag{2}$$

where K is a constant, M is the molecular weight of the protein and A_2 is the second virial coefficient. The K value was determined using a Ca^{2+}/CaM/MLCK peptide complex as a standard sample. In the dilute limit, $R_g(c)$ is given by

$$R_g(c)^2 = R_0^2 - B_{if}c + \ldots, \tag{3}$$

where R_0 is the radius of gyration at infinite dilution and B_{if} is the parameter of interparticle interference (Izumi *et al.*, 1992). Using equations (2) and (3), we estimated the four parameters M, A_2, R_0 and B_{if}. The range of s^2 (Å^{-2}) used for the analysis always satisfies the Guinier condition of $(4\pi^2/3)R_g(c)^2 s^2 < 1$. The second method was that of Kratky, which is defined by the plot of $s^2 I(s, c)$ *versus* s (the Kratky plot), which provides the structural characteristics (*e.g.* molecular shape) of a chain polymer or a biopolymer (Kratky, 1982). For the analysis, all data to $s = 0.06$ Å^{-1} were used.

As a canonical system for the molecular shape, we measured the SAXS data for Ca^{2+}/CaM in the absence of peptide and Ca^{2+}/CaM/MLCK peptide, because it is well known that the former adopts a dumbbell-like structure (Seaton *et al.*, 1985; Heidorn & Trewhella, 1988; Matsushima *et al.*, 1989), while the latter adopts a compact globular structure (Heidorn *et al.*, 1989; Ikura *et al.*, 1992; Meador *et al.*, 1992; Yoshino *et al.*, 1996; Yokouchi *et al.*, 2003). The molecular recognition mode of the Ca^{2+}/CaM/LLP1 complex was analyzed and determined on the basis of a good accordance between the SAXS profile for the Ca^{2+}/CaM/MLCK peptide complex (Hubbard *et al.*, 1988) and the Fourier inversion of the NMR structure of the Ca^{2+}/CaM/MLCK complex (PDB: 1cdl) (Ikura *et al.*, 1992).[1]

3. Results

3.1. Guinier region of the scattering profile

Examples of Guinier plots for a Ca^{2+}/CaM/HV1A2 complex over the concentration series are shown in Fig. 2(a) and (b). In all of the samples studied here except one, there is no evidence of any upward curvature at low s^2 values in the Guinier plots, which indicates that the samples are free from aggregation. A slight upward curvature was observed at low s^2 values in the Ca^{2+}/CaM/HV1rA2Δ10 complex, suggesting the existence of associates. The Fankuchen analysis for this complex (Fankuchen & Jellinek, 1945) indicates that the fraction of the associates is less than 0.01 and therefore can be neglected in the present analysis. The values of $Kc/I(0, c)$ evaluated from the intercepts of the Guinier plots for all samples are shown in Fig. 3 as a function of protein concentration. The plots are linear over the entire concentration range and the value of $[Kc/I(0, c)]_{c=0}$ extrapolated to infinite dilution for each complex has the inverse molecular weight appropriate for the soluble monomer.

The ratio of the molecular weight of the Ca^{2+}/CaM/LLP1 complex to the calculated value, M_{exp}/M_{cal}, and the second virial coefficients, A_2, were calculated using equation (2) and are compiled in Table 1. The values of each ratio are almost 1.0 within the experimental error, indicating that Ca^{2+}/CaM binds each peptide with the molar ratio of 1:1. It is noted that the value of A_2 for the Ca^{2+}/CaM/HV1A2Δ10 complex is positive, while that for the Ca^{2+}/CaM/HV1A2Δ3 complex is almost zero, suggesting that the truncation of residues at the C terminus increases the solubility of the complex. This suggestion is further supported by the fact that the solution of the Ca^{2+}/CaM/HV1A2 complex becomes turbid. Squared radii of gyration at finite

[1] The scattering profile for the Ca^{2+}/CaM/MLCK complex (PDB: 1cdl) was computed using a revised version of the method by Hubbard *et al.* (1988). A close agreement between observed and calculated scattering profiles was obtained.
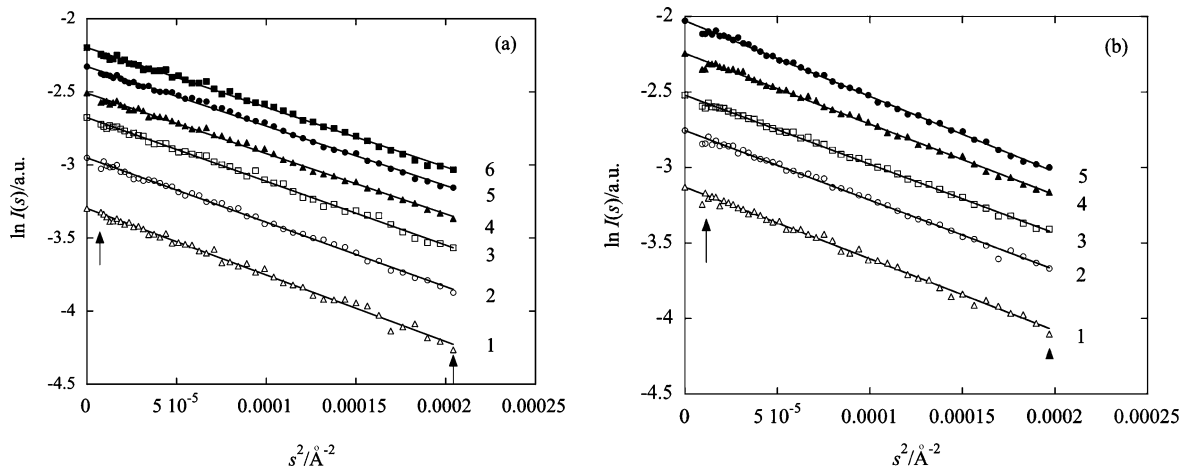
Figure 2
Examples of Guinier plots for Ca^{2+}/CaM/ HV1A2Δ10 complex (a) and Ca^{2+}/CaM/ HV1A2Δ3 complex (b) at various concentrations: (1) 5.0; (2) 7.5; (3) 10.0; (4) 12.5; (5) 15.0; (6) 17.50 mg ml^{-1}.

concentrations, $R_g(c)$, are shown as a function of protein concentration in Fig. 4. Using equation (3), a linear increase with decreasing protein concentration was observed in all complexes except for the Ca^{2+}/CaM/HV1A2Δ3 complex. The slopes of these lines, which arise from interference effects, represent a virial coefficient (Guinier & Fournet, 1955). The values of R_0 and B_{if} are also compiled in Table 1. The R_0 value for the Ca^{2+}/CaM molecule is 21.6 $\pm$ 0.3 Å, a value typical of the dumbbell-shaped structure (Seaton *et al.*, 1985; Heidorn & Trewhella, 1988; Matsushima *et al.*, 1989), while that for the Ca^{2+}/CaM/MLCK peptide complex is 18.0 $\pm$ 0.3 Å at a molar ratio of 1:1, a value typical of the compact globular structure (Yoshino *et al.*, 1996; Yokouchi *et al.*, 2003). The R_0 values for the Ca^{2+}/CaM/LLP1 complexes are intermediate between the two, suggesting that the complexes with LLP1s adopt either a mixture of the dumbbell-shaped structure and the globular structure or a novel structure. The B_{if} value for the Ca^{2+}/CaM/ HV1A2Δ3 complex is negative, suggesting that the interaction is attractive.
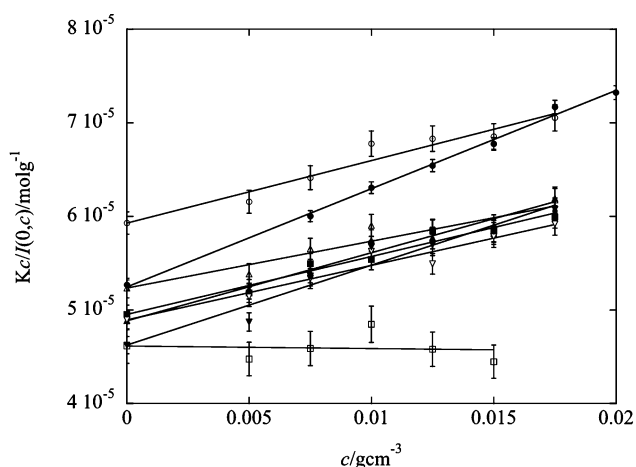

Figure 3
Zimm plots for Ca^{2+}/CaM (open circles), Ca^{2+}/CaM/MLCK peptide complex (filled circles), Ca^{2+}/CaM/HV1A2Δ3 complex (open squares), Ca^{2+}/CaM/HV1A2Δ10 complex (filled squares), Ca^{2+}/CaM/HV1rA2Δ10 complex (open triangles), Ca^{2+}/CaM/HV1B1Δ10 complex (filled triangles), Ca^{2+}/CaM/HV1H2Δ10 complex (open downwards pointing triangles) and Ca^{2+}/CaM/HV1H2WΔ10 complex (filled downwards pointing triangles).

3.2. Kratky region of the scattering profile

Fig. 5(a) shows the Kratky plots for three complexes of Ca^{2+}/CaM/ HV1A2Δ3, Ca^{2+}/CaM/HV1A2Δ10 and Ca^{2+}/CaM/HV1rA2Δ10. For comparison, that for the Ca^{2+}/CaM/MLCK peptide complex is also shown. The data points for the three complexes are almost superimposed on those for the Ca^{2+}/CaM/MLCK peptide complex, indicating that the three complexes adopt almost the same globular structure as that of the Ca^{2+}/CaM/MLCK peptide complex. The results suggest that each HV1A2 also adopts an α-helix in the complex, as the MLCK peptide takes an α-helix in the complex.

Fig. 5(b) shows the Kratky plot for the Ca^{2+}/CaM/HV1B1 complex. For comparison, that for the Ca^{2+}/CaM/MLCK peptide complex is also shown. These data points are almost superimposed, indicating that the Ca^{2+}/CaM/HV1B1 complex adopts almost the same globular structure as that of the Ca^{2+}/CaM/MLCK peptide complex, suggesting that HV1B1 adopts an α-helix in the complex.

Fig. 5(c) shows the Kratky plots for two complexes of Ca^{2+}/CaM/ HV1H2Δ10, and Ca^{2+}/CaM/HV1H2WΔ10. For comparison, that for the Ca^{2+}/CaM/MLCK peptide complex is also shown. These data points are almost superimposed, indicating that the two complexes adopt almost the same globular structure as that of the Ca^{2+}/CaM/ MLCK peptide complex, suggesting that HV1H2 adopts an α-helix in the complex.

4. Discussion

The results for the SAXS measurements presented here show that Ca^{2+}/CaM binds each LLP1 at a molar ratio of 1:1 and each complex adopts almost the same globular structure as that for the Ca^{2+}/CaM/ MLCK peptide complex, suggesting that each LLP1 adopts an α-helix in the complex and that the binding mode of Ca^{2+}/CaM for the LLP1s is almost the same as the MLCK peptides (Srinivas *et al.*, 1993). Comparison between the Ca^{2+}/CaM/HV1A2Δ3 complex and the Ca^{2+}/CaM/HV1A2Δ10 complex indicates that Ca^{2+}/CaM recognizes their common sequence. The sequence comparison of HV1A2Δ10 and MLCK peptide indicates the region of best fit among these peptides, with exact or near matches underlined as shown in Fig. 6, as already indicated for HV1H2 by Micoli *et al.* (2000).

For the case where the binding mode of Ca^{2+}/CaM for the LLP1s is almost the same as the MLCK peptides, a prediction based on a three-dimensional modeling has been carried out (Micoli *et al.*, 2000).
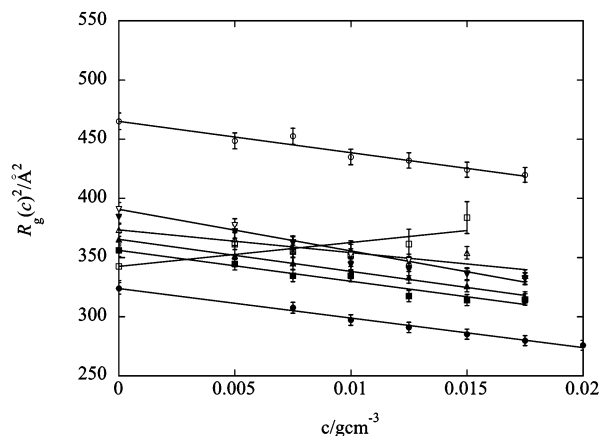
Figure 4
The square of the radius of gyration, R_g^2, for Ca^{2+}/CaM (open circles), Ca^{2+}/CaM/MLCK peptide complex (filled circles), Ca^{2+}/CaM/HV1A2Δ3 complex (open squares), Ca^{2+}/CaM/HV1A2Δ10 complex (filled squares), Ca^{2+}/CaM/HV1rA2Δ10 complex (open triangles), Ca^{2+}/CaM/HV1B1Δ10 complex (filled triangles), Ca^{2+}/CaM/HV1H2Δ10 complex (open downwards pointing triangles) and Ca^{2+}/CaM/HV1H2WΔ10 complex (filled downwards pointing triangles).

That is, an Ala 7 mutation to Trp in the HV1H2Δ10 peptide is predicted to be a substitution that will maximally affect binding to CaM, because this Ala fits in a tight hydrophobic pocket of CaM. Substitution of Trp for Ala is not predicted to change the overall conformation of the LLP1 peptide but is predicted to disrupt binding to CaM, because the large side chain would be within 2 Å of five hydrophobic residues on CaM, too close to allow binding. As a result, the Ca^{2+}/CaM/HV1H2WΔ10 complex cannot adopt almost the same structure as that of the Ca^{2+}/CaM/MLCK complex. However, the actual complex adopts almost the same globular structure as that of the Ca^{2+}/CaM/MLCK complex. The present result strongly suggests that Ca^{2+}/CaM cannot bind HV1H2WΔ10 with the same sequence as that of MLCK. Furthermore, any CaM-binding motif is not retrieved using the CaM target database based on the known binding motifs (Yap *et al.*, 2000).

Therefore, we noted that Ca^{2+}/CaM also binds HV1rA2Δ10 bearing a reverse sequence of HV1A2Δ10 and adopts almost the same globular structure as that observed for the Ca^{2+}/CaM/HV1A2Δ10 complex. Furthermore, the sequence comparison of the HV1rA2Δ10 peptide and the MLCK peptides indicates that both the peptide polarity and the position of conserved hydrophobic residues agree well with each other. The result shows that HV1A2Δ10 binds Ca^{2+}/CaM in the opposite orientation to that observed for the Ca^{2+}/CaM/MLCK complex (Ikura *et al.*, 1992; Meador *et al.*, 1992). In the Ca^{2+}/CaM/MLCK complex, the peptide helix is oriented in one direction such that the N-terminal portion binds to the C-terminal lobe of CaM, while the C-terminal portion binds to the N-terminal lobe of CaM. On the other hand, the present peptide orientation is reversed in the case of the Ca^{2+}/CaM/HV1A2Δ10 complex. As the sequence of the HV1A2Δ10 peptide is almost the same as those of HV1B1Δ10 and HV1H2Δ10, the same logic is applied to these peptides. Thus, the present result suggests that the LLP1s bind Ca^{2+}/CaM in the opposite orientation to that observed for the Ca^{2+}/CaM/MLCK complex and the binding mode is the reverse 1–5–8–14.

Next we discuss the difference in R_0 values listed in Table 1 and the Kratky plots. The structure predicted from the R_0 values suggests that the complexes with LLP1s adopt either a mixture of the dumbbell-shaped structure and the globular structure or a novel structure. On the other hand, the results of the Kratky plots indicate that the Ca^{2+}/

CaM/LLP1 peptide complex adopts almost the same globular shape as that of the Ca^{2+}/CaM/MLCK peptide complex. However, if examined in detail, there is a slight but significant difference in these Kratky plots shown in Fig. 5, indicating that these complexes are not regarded as the same structure but regarded as almost the same structure. The difference may suggest the possibility that the complex with the opposite polarity adopts a novel structure. A more detailed modeling study is necessary to confirm this point. Research is in progress along this line.

Finally, we discuss the difference in the R_0 values listed in Table 1. We noted the difference of the peptide sequence, because only the peptide sequence is different among these complexes. It is well known that the most important factor in the formation of helices of a peptide segment is the average hydrophobicity $\langle H \rangle$ (Mitaku & Hirokawa, 1999). The average hydrophobicity was evaluated by the *SOSUI* system (Hirokawa *et al.*, 1998). The R_0 values listed in Table 1 can be closely connected with $\langle H \rangle$, i.e. $R_0 = 20.66_7 + 3.06_5\langle H \rangle$, $r = 0.96_2$, in which r is the correlation coefficient. The result is consistent with the present suggestion that the peptide adopts an α-helix in the complex.

Schematic models of the Ca^{2+}/CaM/MLCK peptide complex and the Ca^{2+}/CaM/LLP1 peptide complex are shown in Fig. 6.

Figure 5
(a) Kratky plots for Ca^{2+}/CaM (red), Ca^{2+}/CaM/MLCK peptide (black) complex, Ca^{2+}/CaM/HV1A2Δ3 complex (blue), Ca^{2+}/CaM/HV1A2Δ10 complex (green), Ca^{2+}/CaM/HV1rA2Δ10 complex (magenta). (b) Kratky plots for Ca^{2+}/CaM (red), Ca^{2+}/CaM/MLCK peptide (black) complex, Ca^{2+}/CaM/HV1B1Δ10 complex (blue). (c) Kratky plots for Ca^{2+}/CaM (red), Ca^{2+}/CaM/MLCK peptide (black) complex, Ca^{2+}/CaM/HV1H2Δ10 complex (blue), Ca^{2+}/CaM/HV1H2WΔ10 complex (green).
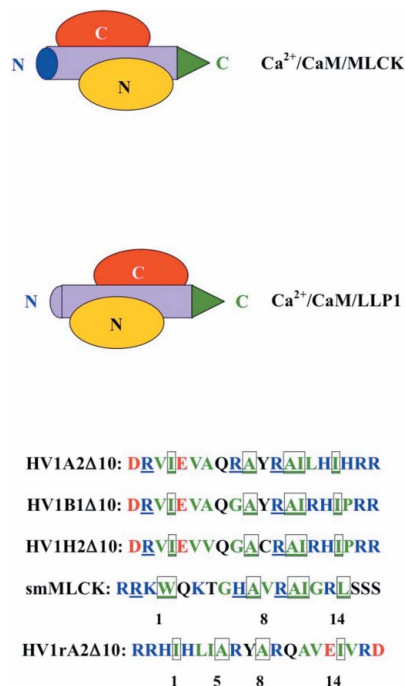
Figure 6
Schematic models of Ca^{2+}/CaM/MLCK peptide complex and Ca^{2+}/CaM/LLP1 complex. N- and C-terminal lobes of Ca^{2+}/CaM are shown in orange and red, respectively. N- and C-terminal termini of the target peptide are shown in blue and green, respectively. The region of best fit between LLP1 and smMLCK peptide is shown, with exact or near matches underlined. The boxed letter represents the position of conserved hydrophobic residues.

5. Conclusions

The SAXS results provide evidence that the CaM-binding domain close to the C terminus of gp160 can bind the N- and C-terminal lobes of CaM with a polarity opposite to that observed for the CaM–MLCK complex. The results suggest that the binding mode of Ca^{2+}/CaM molecular recognition is well preserved despite the sequence variation observed in nature, suggesting that this region of the transmembrane glycoprotein is important to viral replication. Moreover, a revised version of the CaM target database is necessary to retrieve the molecular recognition motif in the opposite orientation.

References

Fankuchen, I. & Jellinek, M. (1945). *Ind. Eng. Chem.* **37**, 158–163.
Guinier, A. & Fournet, G. (1955). *Small-Angle Scattering of X-rays*, pp. 126–133. New York: Wiley.
Hayashi, N., Matsubara, M., Takasaki, A., Titani, K. & Taniguchi, H. (1998). *Protein Expr. Purif.* **12**, 25–28.
Heidorn, D. B., Seeger, P. A., Rokop, S. E., Blumenthal, D. K., Means, A. R., Crepsi, H. & Trewhella, J. (1989). *Biochemistry*, **28**, 6757–6764.
Heidorn, D. B. & Trewhella, J. (1988). *Biochemistry*, **27**, 909–915.
Hirokawa, T., Boon-Chieng, S. & Mitaku, S. (1998). *Bioinformatics*, **14**, 378–379.
Hubbard, S. R., Hodgdon, K. O. & Doniach, S. (1988). *J. Biol. Chem.* **263**, 4151–4158.
Ikura, M., Clore, G. M., Gronenborn, A. M., Zhu, G., Klee, C. B. & Bax, A. (1992). *Science*, **256**, 632–638.
Izumi, Y., Kuwamoto, S., Jinbo, Y. & Yoshino, H. (2001). *FEBS Lett.* **495**, 126–130.
Izumi, Y., Wakita, M., Yoshino, H. & Matsushima, N. (1992). *Biochemistry*, **31**, 12266–12271.
Kratky, O. (1982). *Small-Angle X-ray Scattering*, edited by O. Glatter & O. Kratky, pp. 361–386. London: Academic Press.
Lowry, O. H., Rosebrough, N. J., Farr, A. L. & Randall, R. J. (1951). *J. Biol. Chem.* **193**, 265–275.
Matsushima, N., Izumi, Y., Matsuo, T., Yoshino, H., Ueki, T. & Miyake, Y. (1989). *J. Biochem.* **105**, 883–887.
Meador, W. E., Means, A. R. & Quiocho, F. A. (1992). *Science*, **257**, 1251–1255.
Micoli, K. J., Pan, G., Wu, Y., Williams, J. P., Cook, W. J. & McDonald, J. M. (2000). *J. Biol. Chem.* **275**, 1233–1240.
Miller, M. A., Cloyd, M. W., Liebmann, J., Rinaldo, C. R., Islam, K. R., Wang, S. Z. S., Mietzner, T. A. & Montelaro, R. C. (1993). *Virology*, **196**, 89–100.
Miller, M. A., Garry, R. F., Jaynes, G. J. & Montelaro, R. C. (1991). *AIDS Res. Hum. Retrovir.* **7**, 511–519.
Mitaku, S. & Hirokawa, T. (1999). *Protein Eng.* **12**, 953–957.
Seaton, B. A., Head, J. F., Engelman, D. M. & Richards, F. M. (1985). *Biochemistry*, **24**, 6740–6743.
Srinivas, S. K., Srinivas, R. V., Ananthramaiah, G. M., Compans, R. W. & Segrest, J. P. (1993). *J. Biol. Chem.* **268**, 22895–22899.
Tencza, S. B., Mietzner, T. A. & Montelaro, R. C. (1997). *AIDS Res. Hum. Retrovir.* **13**, 263–269.
Ueki, T., Hiragi, Y., Kataoka, M., Inoko, Y., Amemiya, Y., Izumi, Y., Tagawa, H. & Muroga, Y. (1985). *Biophys. Chem.* **23**, 115–124.
Yap, K. L., Kim, J., Truong, K., Sherman, M., Yuan, T. & Ikura, M. (2000). *J. Struct. Funct. Genom.* **1**, 8–14.
Yokouchi, T., Nogami, H., Izumi, Y., Yoshino, H., Nakashima, K. & Yazawa, M. (2003). *Biochemistry*, **42**, 2195–2201.
Yoshino, H., Izumi, Y., Sakai, K., Takezawa, H., Matsuura, I., Maekawa, H. & Yazawa, M. (1996). *Biochemistry*, **35**, 2388–2393.